Journal of Alloys and Compounds 901 (2022) 163717

Contents lists available at ScienceDirect

Journal of Alloys and Compounds

journal homepage: www.elsevier.com/locate/jalcom

Research Article

Microstructures and mechanical properties of Zr-based metallic glass ablated by nanosecond pulsed laser in various gas atmospheres

Yongfeng Qian[a], Minqiang Jiang[b,c], Zhiyu Zhang[d], Hu Huang[a,*], Jing Hong[a], Jiwang Yan[e]

[a] Key Laboratory of CNC Equipment Reliability, Ministry of Education, School of Mechanical and Aerospace Engineering, Electron Microscopy Center, Jilin University, Changchun, Jilin 130022, China
[b] State Key Laboratory of Nonlinear Mechanics, Institute of Mechanics, Chinese Academy of Sciences, Beijing 100190, China
[c] School of Engineering Science, University of Chinese Academy of Sciences, Beijing 100049, China
[d] Key Laboratory of Optical System Advanced Manufacturing Technology, Changchun Institute of Optics, Fine Mechanics and Physics, Chinese Academy of Sciences, Changchun, China
[e] Department of Mechanical Engineering, Faculty of Science and Technology, Keio University, Yokohama 223-8522, Japan

ARTICLE INFO

Article history:
Received 30 November 2021
Received in revised form 6 January 2022
Accepted 7 January 2022
Available online 10 January 2022

Keywords:
Metallic glass
Laser ablation
Mechanical property
Different atmospheres

ABSTRACT

The surface with micro-convex prepared by laser ablation is beneficial to improving the functional properties of metallic glasses (MGs). However, accompanied by the formation of micro-convex, surface hardness of the ablated area generally decreases due to the softening effect caused by laser thermal shock. Previous studies have shown that the mechanical properties of laser-ablated MG surface are significantly different when using different gas atmospheres. In this study, a comparative investigation was performed to analyze the influence of gas atmosphere (i.e. argon, nitrogen, and air) on the formation of micro-convex as well as its surface characteristics and mechanical properties. Experimental results showed that the atmosphere type did not affect the formation of micro-convex, but significantly affected the surface morphology and element composition of the laser-ablated area. The element analysis and Raman spectral measurements indicated that laser ablation in nitrogen or air atmosphere resulted in local nitridation or oxidation. The results of nanoindentation tests demonstrated that laser ablation in nitrogen or air atmosphere also resulted in surface hardness inhomogeneity, i.e., softening and hardening effects coexist in the ablated area, which could be attributed to the combined influence of laser thermal shock, the introduction of secondary phase as well as laser ablation induced loose structure.

1. Introduction

Due to their unique physical and mechanical properties [1–6], metallic glasses (MGs) are identified as ideal candidates for many engineering applications such as wastewater remediation [7,8], micro-geared motor parts [9] and electronics [10]. However, the practical applications of MGs are impeded by their inherent brittleness [11,12] and size limitation [13]. To overcome the above restrictions, in the past few decades, laser processing techniques such as laser shock peening and laser additive manufacturing have been extensively used to process MGs. For instance, by laser shock peening, compressive residual stress could be introduced into MGs, resulting in the enhancement in plasticity [14–16]. Through laser additive manufacturing, the dimensions of MGs could be effectively increased [17–21]. In addition to these two typical laser processing techniques, laser surface patterning as a kind of surface modification technology is also introduced into the field of MGs to further enhance their functional applications, such as wettability control [22–24] and improving the cytocompatibility [25]. During the laser ablation process, the MG surface is rapidly heated and then cooled; along with this process, a variety of surface micro/nano-structures could be formed, depending on the laser parameters and ablation environment. The typical micro/nano-structures obtained so far include the micro-concave [23,26], groove structure [23,27], ripples [28–30], and metallic glass nanoparticles (MG-NPs) [31–33]. Moreover, our recent work [34] reported that when the Zr-based MG was ablated in argon atmosphere by nanosecond pulsed laser, regular micro-convex could be generated on the MG surface within a certain range of ablation parameters. Previous studies [35,36] indicated that the surfaces with micro-convex were beneficial to improving the tribological performance of materials. In particular, compared with traditional metal alloys, the introduction of laser ablation induced

* Corresponding author.
E-mail address: huanghu@jlu.edu.cn (H. Huang).

https://doi.org/10.1016/j.jallcom.2022.163717
0925-8388/

micro-convex on the surface of MGs may be more beneficial for improving the wear-resistance performance due to their long-range disordered atomic arrangement. However, unfortunately, it has been reported that the hardness of the laser-ablated area is usually lower than that of the as-cast MG surface, due to the softening effect caused by laser thermal shock [37,38]. This is a significant shortcoming of laser processing of MGs, which may hinder its wide applications. Therefore, it is urgently required to develop new strategies for fabricating the micro-convex without sacrificing the surface hardness of MGs.

Previous studies [37,39] indicated that the employed gas atmosphere would affect the final mechanical properties of laser-ablated Zr-based MG surface. Compared to laser ablation in argon atmosphere, laser ablation in nitrogen atmosphere is an effective method to improve the surface hardness of Zr-based MG. This is due to the chemical reaction between the Zr-based MG and nitrogen, inducing the formation of ZrN phase [37]. According to the previous study [37], the introduction of ZrN phase into Zr-based MG can improve its resistance to plastic deformation. On the other hand, ZrN phase has higher hardness compared to the Zr-based MG. These two reasons lead to the surface hardening of Zr-based MG after laser ablation in nitrogen atmosphere. Similarly, the elements in air such as oxygen and nitrogen also have good affinity with the Zr element, which would also induce the formation of oxide and nitride, and thus harden the Zr-based MG surface. Compared to argon and nitrogen atmospheres, nanosecond pulsed laser ablation in air atmosphere is not only economical, but also more convenient. Therefore, a comparative investigation of the influence of gas atmosphere on the formation of micro-convex as well as its surface characteristics and mechanical properties is meaningful.

Accordingly, in this study, the Zr-based MG was ablated by nanosecond pulsed laser in three different atmospheres, i.e. argon, nitrogen and air. Experimental results indicated that micro-convex could be formed under different atmospheres, but their surface morphology and element composition were quite different. The surface hardness of the area after laser ablation in different atmospheres was comparatively evaluated by nanoindentation testing. Finally, the relationship among the surface hardness, chemical composition, and surface microstructure was discussed.

2. Experimental details

2.1. Material

A typical bulk Zr-based MG sample known as Vit 1 ($Zr_{41.2}Ti_{13.8}Cu_{12.5}Ni_{10}Be_{22.5}$) with the dimension of 20 mm × 20 mm × 2 mm was used in this study. Before laser ablation, the sample surface was mechanically ground and polished to be mirror surface with a roughness of about 10 nm.

2.2. Laser ablation process

Ablation experiments were performed by a fiber nanosecond pulsed laser system (SP-050P-A-EP-Z-F-Y, SPI Lasers, UK) with a Gaussian energy distribution. Fig. 1 presents the schematic diagram of the laser ablation process. The laser wavelength, pulse duration, repetition frequency and beam diameter were 1064 nm, 7 ns, 800 kHz and ~ 43 μm, respectively. In order to obtain a relatively flat top of the micro-convex for subsequent testing of surface hardness, the number of laser pulses and the peak laser power intensity were set to be 800 and 7.5×10^{11} W/m^2, respectively, according to our previous study [34]. Three different atmospheres, i.e. air, high purity argon and nitrogen (> 99.999%), were used to investigate the influence of gas atmosphere on the formation of micro-convex and its surface characteristics. The gas pressure was kept the same when using nitrogen and argon atmospheres (0.01 MPa).

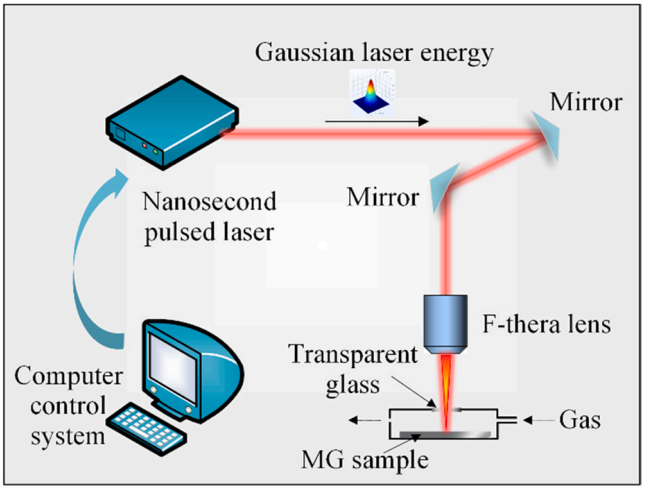

Fig. 1. The schematic diagram of the laser ablation process.

2.3. Characterization of surface microstructure and hardness

Surface microstructures of the laser-ablated areas were observed by a laser scanning confocal microscope (LSCM, OLS4100, Olympus, Japan), an optical microscopy (OM, DSX500, Olympus, Japan) operated at the differential interference mode, and a tungsten filament scanning electron microscopy (SEM, JSM-IT500A, JEOL, Japan) with an acceleration voltage of 10 kV. The chemical compositions of the ablated areas were analyzed by an energy dispersive X-ray spectrometer (EDS, EX-74600U4L2Q, JEOL, Japan) with an acceleration voltage of 15 kV and a working distance of 9.9 mm, a Raman microspectrometer (DXR3, Thermo Fisher Scientific, USA) with a laser wavelength of 532 nm, as well as a X-ray diffractometer (XRD, D8 Advance, Bruker, Germany). Furthermore, surface hardness of the ablated areas was measured at room temperature by a nanoindentation instrument (DUH-211, SHIMADZU, Japan) equipped with a pyramidal indenter. The load-control mode was employed, and the maximum indentation load, loading rate, and dwelling time were 30 mN, 10 mN/s and 5 s, respectively. To ensure the reliability and repeatability of the experimental results, five laser ablation experiments were performed under each gas atmosphere, and the average hardness was obtained after testing in five different laser-ablated areas.

3. Results

3.1. Surface microstructures

Fig. 2 shows the optical and SEM morphologies of the laser-ablated areas obtained in argon (Figs. 2(a) and (b)), nitrogen (Figs. 2(c–e)), and air atmospheres (Figs. 2(f–h)). The number of laser pulses and peak laser power intensity are 800 and 7.5×10^{11} W/m^2, respectively. In Figs. 2(a) and (b), it is seen that a smooth circular ablated area appears on the MG surface after laser ablation in argon atmosphere. In contrast, for laser ablation in nitrogen atmosphere, a cluster of dark material with a diameter of about 40 μm was formed near the center of the ablated area as shown in Fig. 2(c). Furthermore, as shown in Figs. 2(d) and (e), there are some random wrinkles around the cluster, which indicates that thermomechanical disturbance may take place in this region during the ablation process [40,41]. When the gas atmosphere is changed to air, more severe ablation occurs on the MG surface, as evidenced by a large number of residual nano-particles and more remarkable wrinkles as shown in Figs. 2(f–h). Figs. 3(a), (c) and (e) present the three-dimensional (3D) topographies of the laser-ablated areas corresponding to

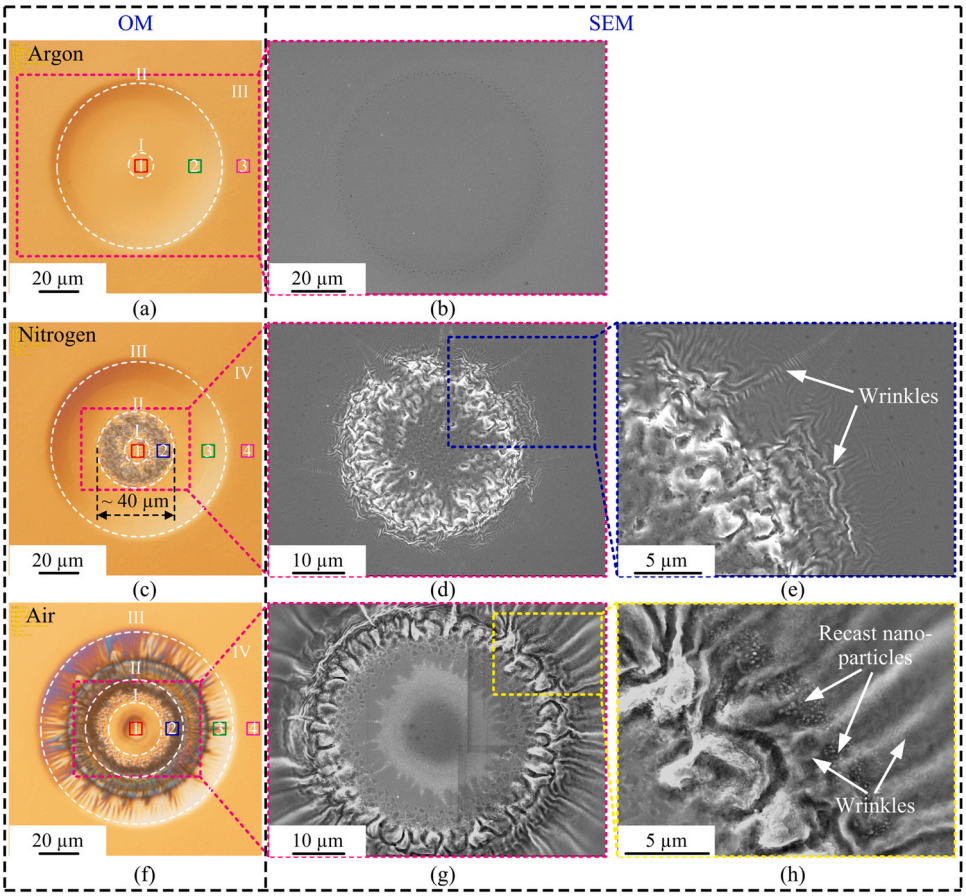

Fig. 2. Optical and SEM morphologies of the laser-ablated areas obtained in three different gas atmospheres: (a) and (b) argon atmosphere; (c–e) nitrogen atmosphere; (f–h) air atmosphere. The number of laser pulses and peak laser power intensity are 800 and 7.5×10^{11} W/m^2, respectively.

Figs. 2(a), (c) and (f), respectively, and the corresponding cross-sectional profiles are illustrated in Figs. 3(b), (d) and (f). It is seen that the micro-convex has been formed in all three atmospheres. Furthermore, the micro-convex formed by laser ablation in air atmosphere has the largest height and diameter, followed by nitrogen and argon. This is due to that the transmittance of the laser in air atmosphere is higher than that of high purity nitrogen and argon. Therefore, when the peak laser power intensity is kept the same, more energy is delivered to the MG surface for laser ablation in air atmosphere, resulting in a more severe ablation, and correspondingly, the micro-convex with a larger dimension is generated. The above results demonstrate that although the formation of micro-convex is independent of the atmosphere, the surface morphology of the ablated area is quite different when using different atmospheres.

3.2. Characterization of chemical composition

As shown in Fig. 2, for the ablated areas obtained in nitrogen and air atmospheres, the surface color shows a significant difference from the center to the outside, suggesting that the chemical composition in these regions may be different. Accordingly, several spots are selected to characterize the chemical composition as shown in Figs. 2(c) and (f), namely spot 1 (central region I), spot 2 (dark region II), spot 3 (edge region III), and spot 4 (non-ablation region IV). For comparison, in Fig. 2(a), the area ablated in argon atmosphere is also divided into three regions, i.e. central region I, edge region II and non-ablation III, and three points are also sequentially selected from the above defined regions. EDS point analysis is used to determine the element composition of different spots in the ablated areas, and Tables 1, 2 and 3 give the corresponding results, respectively. The Be element contained in the sample is not detected due to its small density. The very slight difference in element composition of three different spots marked in Fig. 2(a) (see Table 1) reveals that laser ablation in argon atmosphere does not result in enrichment or segregation of elements. In contrast, in Table 2, for spots 1 and 2, the N element is newly introduced into the central and dark regions after laser ablation in nitrogen atmosphere. Nevertheless, the atomic percent of N element in the edge region is zero as reflected by spot 3. As for laser ablation of MG in the air atmosphere, the O element is detected at every selected spot, as shown in Table 3. At the same time, the atomic percent of O element in the central and dark regions are higher than that in the edge and non-ablation regions.

From the EDS analysis, it is noted that the N and O elements have been introduced into the MG surface when laser ablation is performed in nitrogen and air atmospheres, which would change the phase composition of the laser-ablated areas. To verify this, Raman spectral measurements are performed on the spots mentioned above, and Figs. 4(a–c) show the Raman spectral curves of the laser-ablated areas obtained in argon, nitrogen and air atmospheres, respectively. In Fig. 4(a), the Raman spectral curves of the three spots are basically the same, and there is no any sharp peak, which further confirms that no chemical reaction occurs during laser ablation of MG in argon atmosphere. However, for the spots 1 and 2 in the area ablated in nitrogen atmosphere, two prominent peaks are observed at 223 and 530 cm^{-1} as shown in Fig. 4(b), which is considered to be the ZrN phase according to some previous literatures [42,43]. In addition, in Fig. 4(b), the Raman spectral curves obtained for the spots 3 and 4 are consistent with those in Fig. 4(a), suggesting that these two regions have not been nitrided. For laser ablation in air atmosphere, the Raman peaks at 635 cm^{-1} are observed for the spots

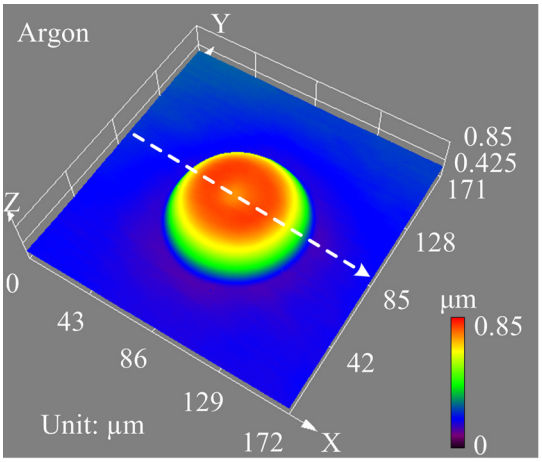

(a)

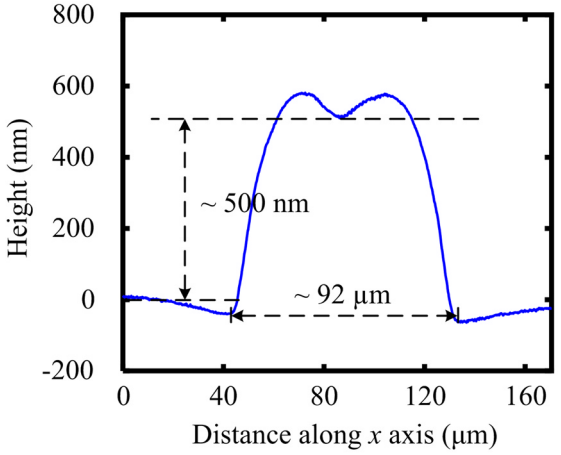

(b)

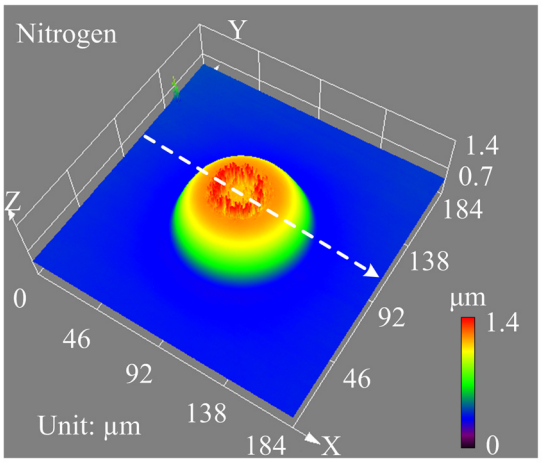

(c)

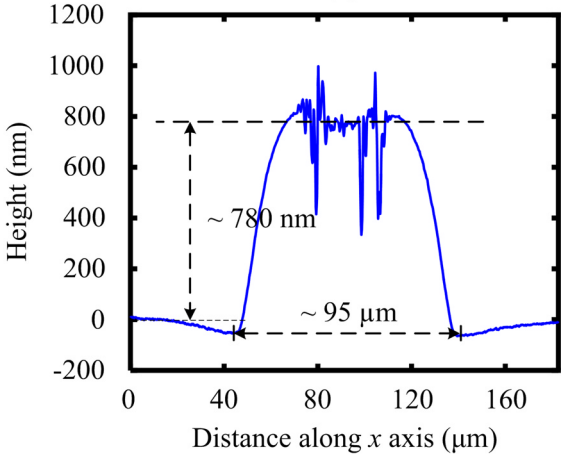

(d)

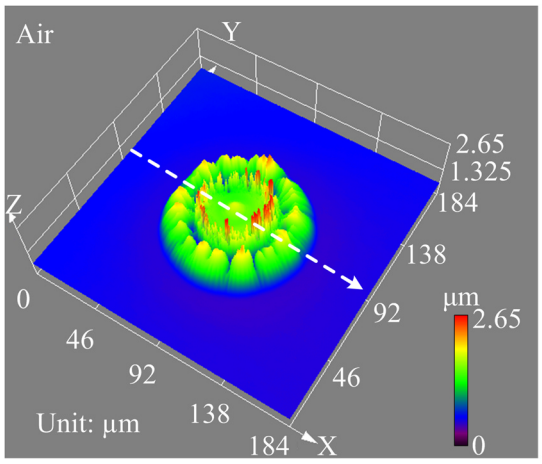

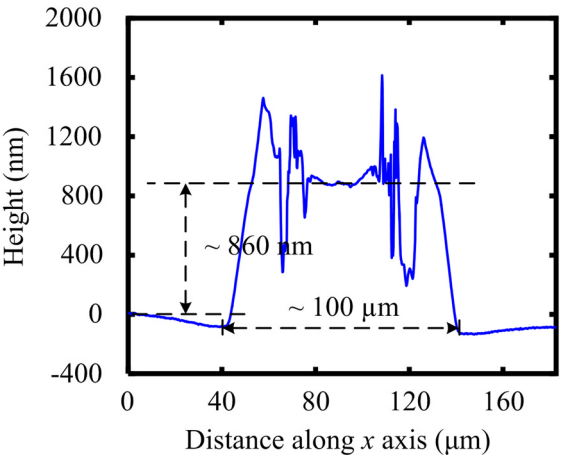

Fig. 3. (a), (c) and (e) present the 3D topographies of the laser-ablated areas corresponding to Figs. 2(a), (c) and (f), respectively. (b), (d) and (f) illustrate the cross-sectional profiles measured along the white dotted lines marked in (a), (c) and (e), respectively.

Table 1
The element composition of the marked spots in Fig. 2(a) (laser ablation in argon atmosphere).

Element	Zr (at%)	Ti (at%)	Cu (at%)	Ni (at%)
Spot 1	54.93	21.04	13.51	10.52
Spot 2	54.83	21.03	13.54	10.59
Spot 3	54.57	21.11	13.93	10.40

Table 2
The element composition of the marked spots in Fig. 2(c) (laser ablation in nitrogen atmosphere).

Element	Zr (at%)	Ti (at%)	Cu (at%)	Ni (at%)	N (at%)
Spot 1	53.54	19.86	10.44	8.28	7.88
Spot 2	48.86	17.49	9.11	7.23	17.30
Spot 3	55.53	20.71	13.52	10.24	0
Spot 4	55.08	20.98	13.31	10.63	0

Table 3
The element composition of the marked spots in Fig. 2(f) (laser ablation in air atmosphere).

Element	Zr (at%)	Ti (at%)	Cu (at%)	Ni (at%)	O (at%)
Spot 1	49.51	15.13	5.46	4.94	24.96
Spot 2	29.97	12.02	9.32	6.30	42.39
Spot 3	49.31	18.76	12.22	9.16	10.55
Spot 4	50.98	19.31	12.72	9.50	7.49

1 and 2 as shown in Fig. 4(c), corresponding to the ZrO_2 phase [44]. Meanwhile, being similar to the results in Fig. 4(b), the crystalline phase also does not exist at the edge and non-ablation regions. In addition, it is noted that although the content of nitrogen element in air is very high, there is no crystalline peak of nitride on the Raman spectral curves, which may be due to that oxidation is dominant during the formation of crystalline phases [45–47]. From the results of EDS point analysis and Raman spectral measurements, it can be concluded that local nitridation or oxidation occurs during laser ablation of MG in nitrogen or air atmosphere, which results in an inhomogeneous chemical composition of the ablated area.

In order to further verify whether the laser ablation induced micro-convex will change the amorphous characteristic of the MG sample, large-area micro-convex arrays were prepared on the MG surface under different atmospheres, and their surface characteristics were characterized by XRD. Fig. 5 presents the results. Being similar to the large-area micro-convex array obtained in argon atmosphere as well as the originally polished surface, the XRD patterns of the large-area micro-convex arrays obtained in nitrogen and air atmospheres also show a broad hump without any crystalline peaks. This indicates that the content of crystalline phase on the laser-abalted MG surface is quite low, so that it could not be detected by the XRD.

3.3. Nanoindentation hardness

As mentioned in the introduction, the introduction of secondary phase would affect the surface hardness of MG materials. Therefore, to further investigate the influence of gas atmosphere on the surface hardness, nanoindentation tests are carried out at each divided region of the ablated areas. Due to the limited size of some regions, such as the dark region II in Figs. 2(c) and (f), a relatively small indentation load of 30 mN is used to avoid the indenter from penetrating into adjacent regions. The average hardness of different regions obtained in argon, nitrogen and air atmospheres are shown in Figs. 6(a–c), respectively. In Fig. 6(a), the average hardness of the central region I and edge region II are less than that of the non-ablation region III, which can be well explained by the softening effect caused by laser thermal shock [37,38]. In contrast, for laser ablation in nitrogen or air atmosphere, the results in Figs. 6(b) and (c) show that the softening and hardening effects coexist in the ablated area. As shown in Fig. 6(b), after ablation in nitrogen atmosphere, the average hardness of the central region I is 8.11 GPa, which is significantly higher than that of the non-ablation region. However, from the central region I to the dark region II, the average hardness is greatly reduced from 8.11 GPa to 4.33 GPa; while, for the edge region, the average hardness is recovered to 5.47 GPa, which is approximately equal to the average hardness of the area ablated in argon atmosphere. A similar variation trend of average hardness appears in Fig. 6(c), indicating that the effects of nitrogen and air atmospheres on the surface hardness of the ablated areas are basically consistent.

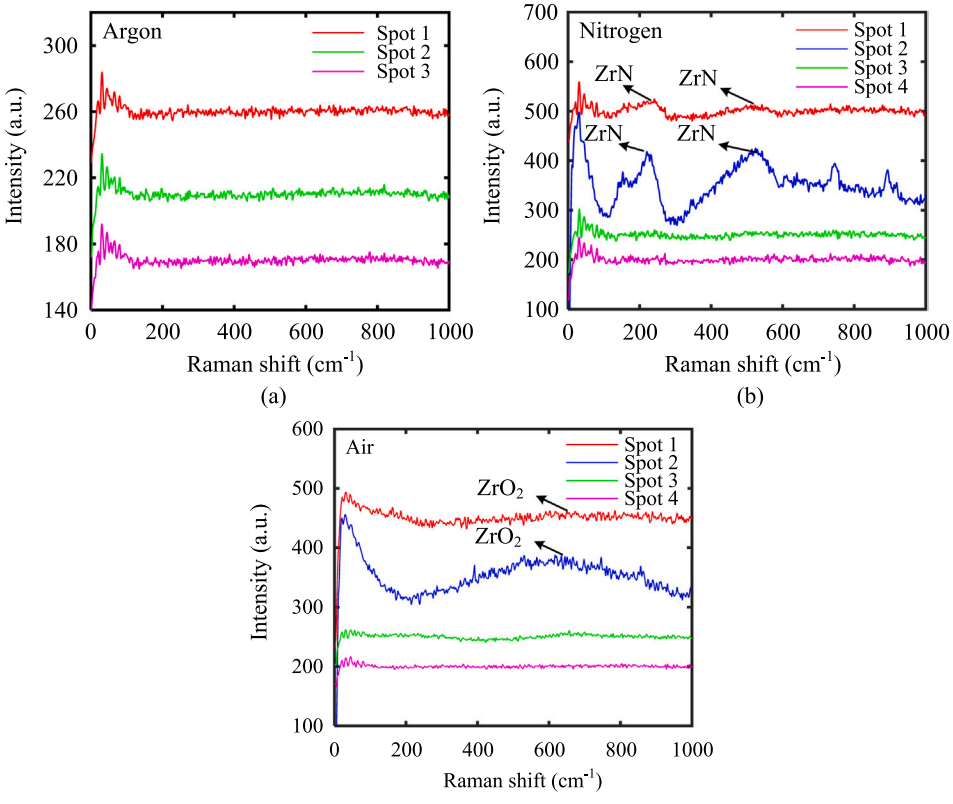

Fig. 4. Raman spectral curves of the different spots obtained in (a) argon, (b) nitrogen, and (c) air atmospheres.

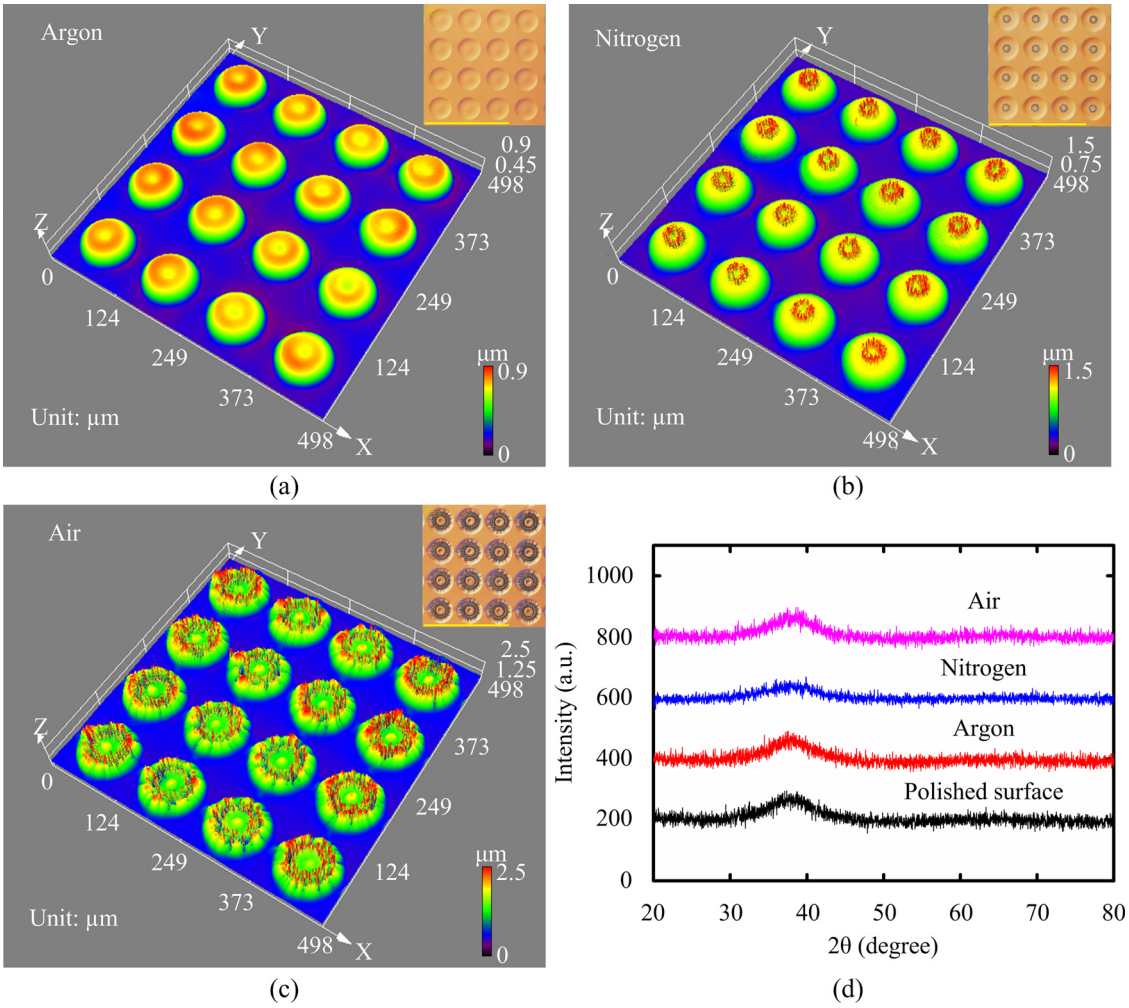

Fig. 5. 3D topographies of the large-area micro-convex arrays obtained in three different gas atmospheres: (a) argon atmosphere, (b) nitrogen atmosphere, and (c) air atmosphere. The number of laser pulses and peak laser power intensity are 800 and 7.5×10^{11} W/m^2, respectively. (d) XRD patterns of the large-area micro-convex arrays obtained in different gas atmospheres as well as the originally polished surface.

4. Discussion

4.1. Effects of gas atmosphere on the chemical composition of the ablated area

The above results indicate that laser ablation in nitrogen or air atmosphere will lead to local nitridation or oxidation of the Zr-based MG. In fact, this local nitridation or oxidation could be attributed to the Gaussian distribution of the laser beam intensity. During laser ablation, the laser energy deposited in different regions is different, resulting in a temperature gradient in the ablated area. Around the center of the ablated area, including the central region I and the dark region II, the temperature is relatively high, so those regions are more likely to be nitrided or oxidized; while the edge region III retains the intrinsic amorphous properties owing to the relatively low temperature. In addition, compared to the edge area III, the central area I and the dark area II are closer to the laser ablation induced high-temperature plasma, which may also promote the nucleation of crystals [31]. It is worth noting that no matter laser ablation is performed in nitrogen or air atmosphere, the degree of nitridation or oxidation in the dark region II is higher than that in the central region I, which is reflected in the higher atomic percent of N or O element in the EDS analysis and more prominent crystalline peak of ZrN or ZrO_2 phase on the Raman spectral curves. Fig. 7 presents the possible reason. As illustrated in Fig. 7, with the role of recoil pressure and the expansion of the plasma plume, the alloy melts in the center of ablated area are squeezed away to form the pileup, and correspondingly, the crystalline phases formed in the central region I will flow radially outward along with the alloy melts. However, during the outward flow of the crystalline phases, the pileup might act as a strong boundary so that the crystalline phases cannot pass through it, leading to the formation of a ring-like accumulation region, i.e. dark regions II as shown in Figs. 2(c) and (f). Meanwhile, the formation of ring-like accumulations will lead to an increase in height of the micro-convex, and this may be one reason why the micro-convex obtained in nitrogen and air atmospheres is higher than that obtained in argon atmosphere. On the other hand, the presence of crystalline phases will affect the flow of the alloy melts during the cooling process, resulting in a significant difference in surface morphology of the laser-ablated areas obtained in three different gas atmospheres.

4.2. Effects of gas atmosphere on the surface hardness distribution of the ablated area

Surface hardness plays an important role in surface engineering applications of MGs. The above results suggest that after laser ablation in argon atmosphere, the whole ablated area exhibits a decreased surface hardness, which could be attributed to the increase in free volume caused by laser thermal shock [48,49]. It is worth

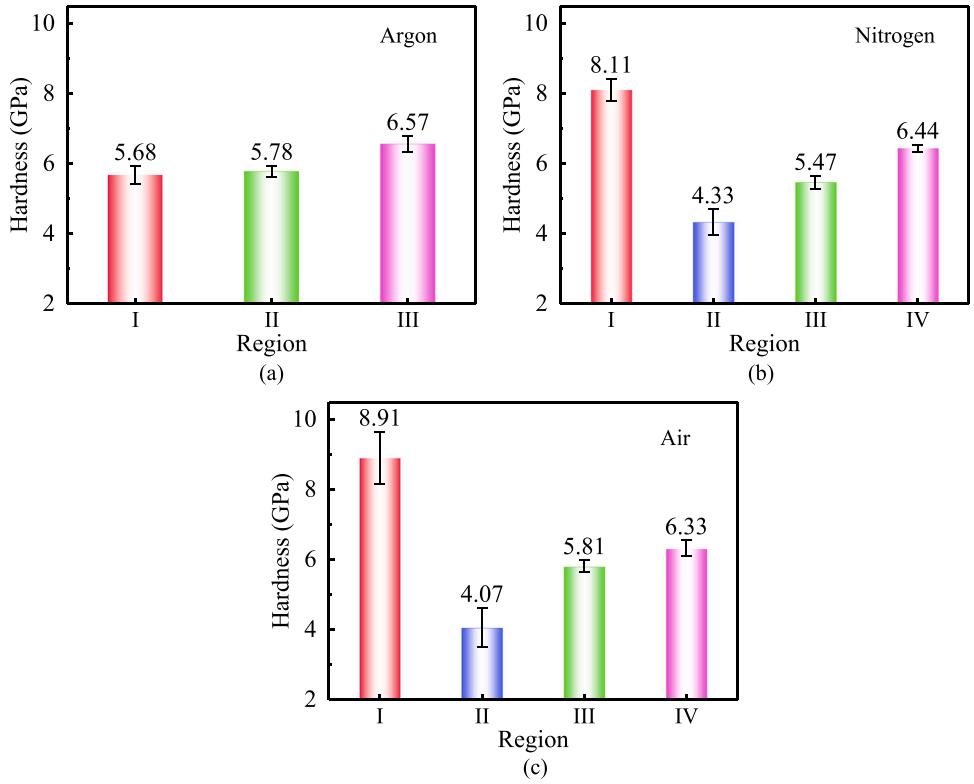

Fig. 6. Nanoindentation hardness measured in the different regions ablated in (a) argon, (b) nitrogen, and (c) air atmospheres.

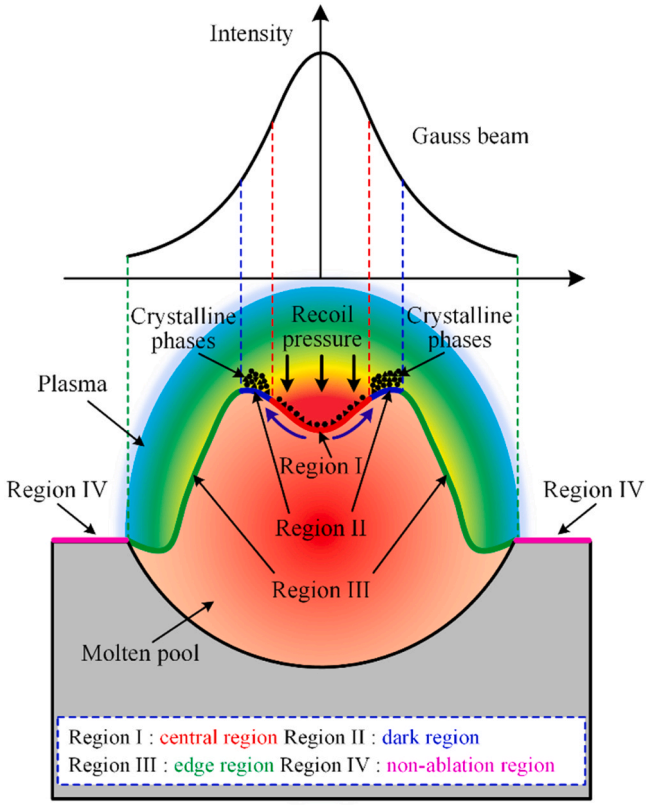

Fig. 7. Schematic diagram illustrating the generation and location of crystalline phases when laser ablation is performed in nitrogen or air atmosphere.

noting that the rapid heating during laser ablation can also lead to surface softening, which is associated with excess stored enthalpy [50]. Compared to the entire softened phenomenon, an interesting finding of this study is that the hardening and softening effects co-exist in the area ablated in nitrogen or air atmosphere, i.e. the dark and edge regions with the hardness lower than the non-ablation region, and the central region with the hardness much higher than the non-ablation region. According to the comparative results of the phase composition, it is clear that the secondary phase has been introduced into some local areas after laser ablation in nitrogen or air atmosphere. Previous studies [37,51] indicate that the introduction of secondary phase into MGs has a positive influence on the surface hardness, i.e. the higher the content of secondary phase, the higher the surface hardness. Accordingly, when laser ablation is performed in nitrogen or air atmosphere, the hardening effect caused by the introduction of secondary phase and the softening effect due to the laser thermal shock compete with each other, determining the final surface hardness. The local hardening and softening observed in this study can be explained by this competitive mechanism. For the central region with a relatively high content of secondary phase, the hardening effect is dominant, leading to the increase in surface hardness; while, for the edge region with a relatively low or even zero content of secondary phase, the softening effect is dominant, resulting in the decrease in surface hardness. However, there is a discrepancy that the dark region with the highest content of secondary phase exhibits the lowest surface hardness. This phenomenon may be due to the difference in the topography between the dark region and other regions. As shown in Figs. 2(d) and (g), compared to other regions, the dark regions display more significant porosity, indicating a loose internal structure. This loose structure will result in a substantial decrease in surface harness. In addition, the laser thermal shock can also lead to softening of this region. In order to further analyze the influence of loose structure on surface hardness in the current study, Figs. 8(a–c) present the representative load-depth curves corresponding to laser-ablated areas obtained in argon, nitrogen and air atmosphere, respectively. It is seen that for region II, the slope of the loading curve changes

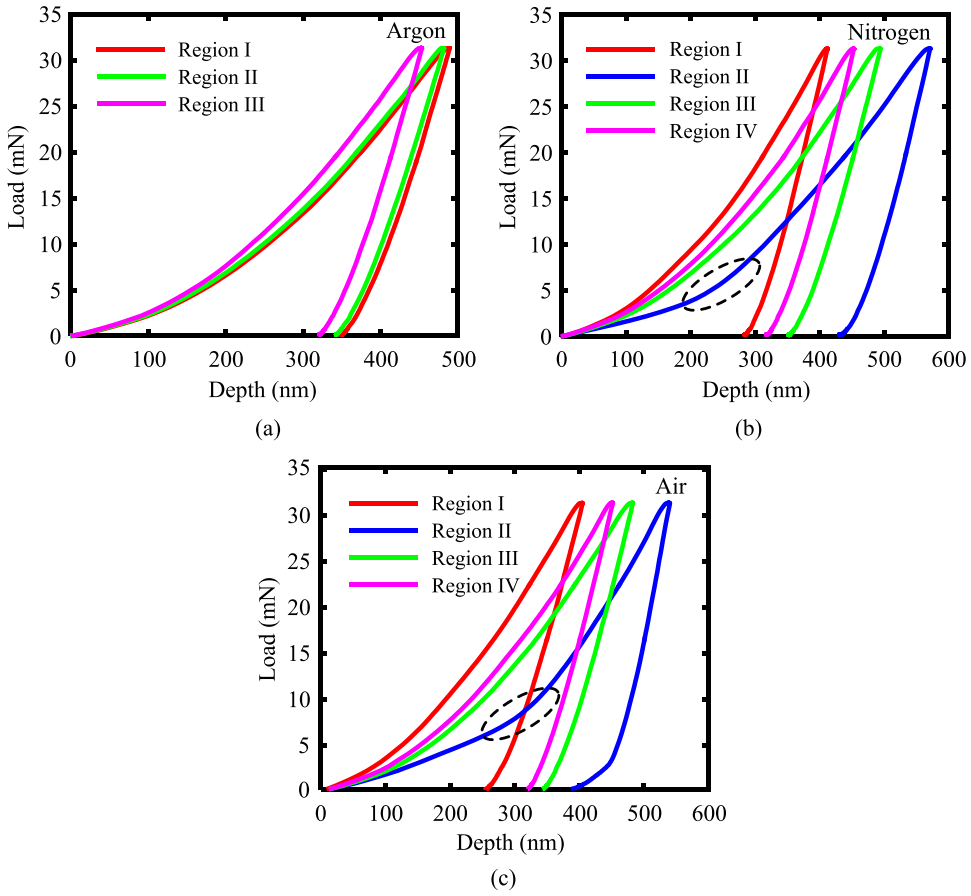

Fig. 8. The representative load-depth curves obtained in the different regions abalted in (a) argon, (b) nitrogen, and (c) air atmospheres.

obviously at a certain point (see Figs. 8(b) and (c)). Before the inflection point, the indentation depth increases rapidly with a slight increase of the indentation load, which confirms the relatively low hardness of the upper loose structure. Therefore, with the combined influence of laser thermal shock, the introduction of secondary phase as well as laser ablation induced loose structure, the area ablated in nitrogen or air atmosphere exhibits a gradient fluctuation in surface hardness.

5. Conclusions

In summary, nanosecond pulsed laser ablation of Zr-based MG was performed in three typical atmospheres (i.e. argon, nitrogen, and air), and the surface microstructures, chemical composition, and nanoindentation hardness of the laser-ablated areas were characterized and comparatively analyzed in detail. The main conclusions are as follows:

(1) For these three different atmospheres, although all laser-ablated areas displayed the micro-convex, their surface morphology and element composition were quite different. The EDS analysis and Raman spectral measurements indicated that local nitridation or oxidation occurred during laser ablation of MG in nitrogen or air atmosphere. Accordingly, the dark region formed after laser ablation in nitrogen or air atmosphere was attributed to the introduction of secondary phase and its flow.
(2) After laser ablation in argon atmosphere, the ablated area showed typical softening. Differently, the surface hardness of the area ablated in nitrogen or air atmosphere exhibited a gradient fluctuation. In the center of the ablation area, the surface hardness was much higher than that of the non-ablation region. From the central region to the dark region, the surface hardness was greatly reduced to much less than that of the non-ablation area, and then its value was slightly increased from the dark region to the edge region, but still less than that of the non-ablation region. This gradient fluctuation in surface hardness was attributed to the combined influence of laser thermal shock, the introduction of secondary phase as well as laser ablation induced loose structure.

This study reveals that the microstructures and mechanical properties of the micro-convex formed after laser ablation are strongly dependent on the employed gas atmosphere. In our future work, the characteristics of sub-micron and nanometer level of laser-ablated areas would be further studied by using the transmission electron microscopy (TEM) when it is available.

CRediT authorship contribution statement

Yongfeng Qian: Investigation, Formal analysis, Data curation, Writing – original draft. **Minqiang Jiang:** Investigation, Methodology. **Zhiyu Zhang:** Data curation, Methodology. **Hu Huang:** Conceptualization, Funding acquisition, Methodology, Resources, Supervision, Writing – review & editing. **Jing Hong:** Investigation. **Jiwang Yan:** Supervision.

Declaration of Competing Interest

The authors declare that they have no known competing financial interests or personal relationships that could have appeared to influence the work reported in this paper.

Acknowledgements

This work was supported by the National Natural Science Foundation of China (Grant Nos. 51705197 and 11972345), the Young Elite Scientists Sponsorship Program by CAST (YESS) (Grant No. 2017QNRC001), the Graduate Innovation Fund of Jilin University (Grant No. 101832020CX106), and the Fundamental Research Funds for the Central Universities (2019-2021).

References

[1] W.H. Wang, Bulk metallic glasses with functional physical properties, Adv. Mater. 21 (2009) 4524–4544.
[2] A. Inoue, N. Nishiyama, New bulk metallic glasses for applications as magnetic-sensing, chemical, and structural materials, MRS Bull. 32 (2007) 651–658.
[3] R. Maaß, K. Samwer, W. Arnold, C.A. Volkert, A single shear band in a metallic glass: local core and wide soft zone, Appl. Phys. Lett. 105 (2014) 171902.
[4] F.L. Zhang, G.W. Huang, J.M. Liu, Z.J. Du, S.X. Wu, C.Y. Wang, Grinding performance and wear of metal bond super-abrasive tools in grinding of Zr-based bulk metallic glass, Int. J. Refract. Met. Hard Mater. 97 (2021) 105501.
[5] V.V. Ozherelyev, A.I. Bocharov, A.V. Bondarev, Y.V. Barmin, X-ray diffraction study of atomic structure of Hf–W amorphous alloys, Int. J. Refract. Met. Hard Mater. 48 (2015) 141–144.
[6] N. Li, Z. Liu, X.Y. Wang, M. Zhang, Vibration-accelerated activation of flow units in a Pd-based bulk metallic glass, Mater. Sci. Eng. A 692 (2017) 62–66.
[7] S.X. Liang, X.Q. Wang, W.C. Zhang, Y.J. Liu, W.M. Wang, L.C. Zhang, Selective laser melting manufactured porous Fe-based metallic glass matrix composite with remarkable catalytic activity and reusability, Appl. Mater. Today 19 (2020) 100543.
[8] L.C. Zhang, Z. Jia, F. Lyu, S.X. Liang, J. Lu, A review of catalytic performance of metallic glasses in wastewater treatment: Recent progress and prospects, Prog. Mater. Sci. 105 (2019) 100576.
[9] A. Inoue, A. Takeuchi, Recent development and application products of bulk glassy alloys, Acta Mater. 59 (2011) 2243–2267.
[10] M. Telford, The case for bulk metallic glass, Mater. Today 7 (2004) 36–43.
[11] R. Maaß, D. Klaumünzer, J.F. Löffler, Propagation dynamics of individual shear bands during inhomogeneous flow in a Zr-based bulk metallic glass, Acta Mater. 59 (2011) 3205–3213.
[12] N. Li, J.J. Zhang, W. Xing, D. Ouyang, L. Liu, 3D printing of Fe-based bulk metallic glass composites with combined high strength and fracture toughness, Mater. Des. 143 (2018) 285–296.
[13] H. Huang, Y.F. Qian, C. Wang, J.W. Yan, Laser induced micro-cracking of Zr-based metallic glass using 10^{11} W/m^2 nano-pulses, Mater. Today Commun. 25 (2020) 101554.
[14] Y.S. Li, K. Zhang, Y. Wang, W.Q. Tang, Y.T. Zhang, B.C. Wei, Z. Hu, Abnormal softening of Ti-metallic glasses during nanosecond laser shock peening, Mater. Sci. Eng. A 773 (2020) 138844.
[15] Y.F. Cao, X. Xie, J. Antonaglia, B. Winiarski, G. Wang, Y.C. Shin, P.J. Withers, K.A. Dahmen, P.K. Liaw, Laser shock peening on Zr-based bulk metallic glass and its effect on plasticity: Experiment and modeling, Sci. Rep. 5 (2015) 10789.
[16] J. Fu, Y.H. Zhu, C. Zheng, R. Liu, Z. Ji, Effect of laser shock peening on the compressive deformation and plastic behavior of Zr-based bulk metallic glass, Opt. Lasers Eng. 86 (2016) 53–61.
[17] X.D. Nong, X.L. Zhou, Y.X. Ren, Fabrication and characterization of Fe-based metallic glasses by selective laser melting, Opt. Laser Technol. 109 (2019) 20–26.
[18] Z. Mahbooba, L. Thorsson, M. Unosson, P. Skoglund, H. West, T. Horn, C. Rock, E. Vogli, O. Harrysson, Additive manufacturing of an iron-based bulk metallic glass larger than the critical casting thickness, Appl. Mater. Today 11 (2018) 264–269.
[19] Y.Y. Shen, Y.Q. Li, C. Chen, H.-L. Tsai, 3D printing of large, complex metallic glass structures, Mater. Des. 117 (2017) 213–222.
[20] Y.Q. Li, Y.Y. Shen, M.C. Leu, H.-L. Tsai, Mechanical properties of Zr-based bulk metallic glass parts fabricated by laser-foil-printing additive manufacturing, Mater. Sci. Eng. A 743 (2019) 404–411.
[21] J.Y. Shi, S.Y. Ma, S. Wei, J.P. Best, M. Stolpe, B. Markert, Connecting structural defects to tensile failure in a 3D-printed fully-amorphous bulk metallic glass, Mater. Sci. Eng. A 813 (2021) 141106.
[22] H. Huang, J.W. Yan, Surface patterning of Zr-based metallic glass by laser irradiation induced selective thermoplastic extrusion in nitrogen gas, J. Micromech. Microeng. 27 (2017) 075007.
[23] Y. Jiao, E. Brousseau, X.J. Shen, X.X. Wang, Q.Q. Han, H.X. Zhu, S. Bigot, W.F. He, Investigations in the fabrication of surface patterns for wettability modification on a Zr-based bulk metallic glass by nanosecond laser surface texturing, J. Mater. Process. Technol. 283 (2020) 116714.
[24] N. Li, T. Xia, L.P. Heng, L. Liu, Superhydrophobic Zr-based metallic glass surface with high adhesive force, Appl. Phys. Lett. 102 (2013) 251603.
[25] Y. Jiao, E. Brousseau, W.N. Ayre, E. Gait-Carr, X.J. Shen, X.X. Wang, S. Bigot, H.X. Zhu, W.F. He, In vitro cytocompatibility of a Zr-based metallic glass modified by laser surface texturing for potential implant applications, Appl. Surf. Sci. 547 (2021) 149194.
[26] E. Williams, E.B. Brousseau, Nanosecond laser processing of $Zr_{41.2}Ti_{13.8}Cu_{12.5}Ni_{10}Be_{22.5}$ with single pulses, J. Mater. Process. Technol. 232 (2016) 34–42.
[27] H. Huang, N. Jun, M.Q. Jiang, M. Ryoko, J.W. Yan, Nanosecond pulsed laser irradiation induced hierarchical micro/nanostructures on Zr-based metallic glass substrate, Mater. Des. 109 (2016) 153–161.
[28] Y. Liu, M.Q. Jiang, G.W. Yang, Y.J. Guan, L.H. Dai, Surface rippling on bulk metallic glass under nanosecond pulse laser ablation, Appl. Phys. Lett. 99 (2011) 191902.
[29] Z. Zhao, B. Zhao, Y. Lei, J.J. Yang, C.L. Guo, Laser-induced regular nanostructure chains within microgrooves of Fe-based metallic glass, Appl. Surf. Sci. 529 (2020) 147156.
[30] Y.H. Lei, J.J. Yang, C. Cong, C.L. Guo, Fabrication of homogenous subwavelength grating structures on metallic glass using double-pulsed femtosecond lasers, Opt. Lasers Eng. 134 (2020) 106273.
[31] S.X. Liang, L.C. Zhang, S. Reichenberger, S. Barcikowski, Design and perspective of amorphous metal nanoparticles from laser synthesis and processing, Phys. Chem. Chem. Phys. 23 (2021) 11121–11154.
[32] S.X. Liang, S. Salamon, S. Zerebecki, L.C. Zhang, Z. Jia, H. Wende, S. Reichenberger, S. Barcikowski, A laser-based synthesis route for magnetic metallic glass nanoparticles, Scr. Mater. 203 (2021) 114094.
[33] Y.F. Qian, H. Huang, M.Q. Jiang, J.W. Yan, Nanosecond pulsed laser-induced formation of nanopattern on Fe-based metallic glass surface, Appl. Surf. Sci. 577 (2022) 151976.
[34] Y.F. Qian, M.Q. Jiang, Z.Y. Zhang, H. Huang, J.W. Yan, On the transformation between micro-concave and micro-convex in nanosecond laser ablation of a Zr-based metallic glass, J. Manuf. Process. 68 (2021) 1114–1122.
[35] L.M. Vilhena, M. Sedlaček, B. Podgornik, J. Vižintin, A. Babnik, J. Možina, Surface texturing by pulsed Nd:YAG laser, Tribol. Int. 42 (2009) 1496–1504.
[36] J. Tong, J.Y. Sun, D.H. Chen, S.J. Zhang, Geometrical features and wettability of dung beetles and potential biomimetic engineering applications in tillage implements, Soil Till. Res. 80 (2005) 1–12.
[37] H. Huang, M.Q. Jiang, J.W. Yan, The coupling effects of laser thermal shock and surface nitridation on mechanical properties of Zr-based metallic glass, J. Alloy. Compd. 770 (2019) 864–874.
[38] H. Huang, M.Q. Jiang, J.W. Yan, Softening of Zr-based metallic glass induced by nanosecond pulsed laser irradiation, J. Alloy. Compd. 754 (2018) 215–221.
[39] J. Wegner, M. Frey, S. Kleszczynski, R. Busch, G. Witt, Influence of process gas during powder bed fusion with laser beam of Zr-based bulk metallic glasses, Procedia CIRP 94 (2020) 205–210.
[40] S.S. Zeng, Y. Liu, S.L. Li, K.Y. Shen, Z.L. Hou, A.P. Chooi, A.T. Smith, Z. Chen, L.Y. Sun, Smart laser-writable micropatterns with multiscale photo/moisture reconstructible structure, Adv. Funct. Mater. 31 (2020) 2009481.
[41] Y. Liu, M.Q. Jiang, G.W. Yang, J.H. Chen, Y.J. Guan, L.H. Dai, Saffman–Taylor fingering in nanosecond pulse laser ablating bulk metallic glass in water, Intermetallics 31 (2012) 325–329.
[42] J.Y. Li, Y. Sun, Y. Tan, F.M. Xu, X.L. Shi, N. Ren, Zirconium nitride (ZrN) fibers prepared by carbothermal reduction and nitridation of electrospun PVP/zirconium oxychloride composite fibers, Chem. Eng. J. 144 (2008) 149–152.
[43] H. Huang, J. Noguchi, J.W. Yan, Shield gas induced cracks during nanosecond-pulsed laser irradiation of Zr-based metallic glass, Appl. Phys. A 122 (2016) 881.
[44] B. Usmani, V. Vijay, R. Chhibber, A. Dixit, Investigation of ZrO_x/ZrC–ZrN/Zr thin-film structural evolution and their degradation using X-ray diffraction and Raman spectrometry, Appl. Phys. A 122 (2016) 992.
[45] R. Yamada, N. Nomura, J. Saida, A. Kawasaki, Selective oxidation/crystallization and their patterning on metallic glass by laser irradiation, J. Alloy. Compd. 727 (2017) 549–554.
[46] J. Antonowicz, P. Zalden, K. Sokolowski-Tinten, K. Georgarakis, R. Minikayev, A. Pietnoczka, F. Bertram, M. Chaika, M. Chojnacki, P. Dłużewski, K. Fronc, A.L. Greer, C. Jastrzębski, D. Klinger, C. Lemke, O.M. Magnussen, B. Murphy, K. Perumal, U. Ruett, K.J. Warias, R. Sobierajski, Devitrification of thin film Cu–Zr metallic glass via ultrashort pulsed laser annealing, J. Alloy. Compd. 887 (2021) 161437.
[47] L. Liu, K.C. Chan, Oxidation of $Zr_{55}Cu_{30}Al_{10}Ni_5$ bulk metallic glass in the glassy state and the supercooled liquid state, Appl. Phys. A 80 (2005) 1737–1744.
[48] Y.H. Zhu, J. Fu, C. Zheng, Z. Ji, Structural and mechanical modifications induced on Zr-based bulk metallic glass by laser shock peening, Opt. Laser Technol. 86 (2016) 54–60.
[49] Y.H. Zhu, J. Fu, C. Zheng, Z. Ji, Effect of laser shock peening without absorbent coating on the mechanical properties of Zr-based bulk metallic glass, Opt. Laser Technol. 75 (2015) 157–163.
[50] S. Küchemann, P.M. Derlet, C.Y. Liu, D. Rosenthal, G. Sparks, W.S. Larson, R. Maaß, Energy storage in metallic glasses via flash annealing, Adv. Funct. Mater. 28 (2018) 1805385.
[51] N.H. Tariq, B.A. Hasan, J.I. Akhter, Evolution of microstructure in $Zr_{55}Cu_{30}Al_{10}Ni_5$ bulk amorphous alloy by high power pulsed Nd:YAG laser, J. Alloy. Compd. 485 (2009) 212–214.